Direct high-resolution mapping of electrocatalytic activity of semi-two-dimensional catalysts with single-edge sensitivity

Tong Sun^{a,b,1}, Dengchao Wang^{a,1}, Michael V. Mirkin^{a,b,2}, Hao Cheng^{c,d}, Jin-Cheng Zheng^{c,d,2}, Ryan M. Richards^e, Feng Lin (林锋)^f, and Huolin L. Xin^{g,h,2}

^aDepartment of Chemistry and Biochemistry, Queens College, City University of New York, Flushing, NY 11367; ^bChemistry Program, The Graduate Center of the City University of New York, New York, NY 10016; ^cDepartment of Physics, Collaborative Innovation Center for Optoelectronic Semiconductors and Efficient Devices, Xiamen University, 361005 Xiamen, China; ^dInstitute of Artificial Intelligence, Xiamen University Malaysia, 439000 Sepang, Selangor, Malaysia; ^eDepartment of Chemistry, Colorado School of Mines, Golden, CO 80401; ^fDepartment of Physics and Astronomy, University of California, Irvine, CA 92697; and ^bCenter for Functional Nanomaterials, Brookhaven National Laboratory, Upton, NY 11973

Edited by Héctor D. Abruña, Cornell University, Ithaca, NY, and approved April 26, 2019 (received for review December 19, 2018)

The catalytic activity of low-dimensional electrocatalysts is highly dependent on their local atomic structures, particularly those lesscoordinated sites found at edges and corners; therefore, a direct probe of the electrocatalytic current at specified local sites with true nanoscopic resolution has become critically important. Despite the growing availability of operando imaging tools, to date it has not been possible to measure the electrocatalytic activities from individual material edges and directly correlate those with the local structural defects. Herein, we show the possibility of using feedback and generation/collection modes of operation of the scanning electrochemical microscope (SECM) to independently image the topography and local electrocatalytic activity with 15-nm spatial resolution. We employed this operando microscopy technique to map out the oxygen evolution activity of a semi-2D nickel oxide nanosheet. The improved resolution and sensitivity enables us to distinguish the higher activities of the materials' edges from that of the fully coordinated surfaces in operando. The combination of spatially resolved electrochemical information with state-of-the-art electron tomography, that unravels the 3D complexity of the edges, and ab initio calculations allows us to reveal the intricate coordination dependent activity along individual edges of the semi-2D material that is not achievable by other methods. The comparison of the simulated line scans to the experimental data suggests that the catalytic current density at the nanosheet edge is ~200 times higher than that at the NiO basal plane.

scanning electrochemistry \mid oxygen evolution reaction \mid electron tomography

Synthesis and fabrication of material structures rich in catalytic active sites is essential for developing more efficient and less-expensive electrocatalysts. However, much of the progress in this field is limited by the difficulty in pinpointing the active sites particularly when their size is on the atomic scale (1-3). Nickel oxide (NiO), for example, is an efficient oxygen evolution catalyst for water electrolysis. Its oxygen evolution reaction (OER) activity can be significantly improved by making it into nanostructures (4-6), suggesting that the exposure of nanoscale facets/corner and edge sites could be the key contributor to the enhanced activity, but so far there is no direct operando microscopy tool that allows a nanoscale mapping of the electrocatalytic currents on NiO or any other types of electrocatalyst with single-edge, single-corner, or single-nanofacet sensitivity. In particular, to date, the inferences regarding the catalytic advantage of the undercoordinated edge sites of electrocatalysts were typically drawn from bulk surface/ edge correlative measurements. This type of bulk inference experiment works remarkably well for simple systems, such as singlelayered MoS2, where the surface area and the circumference have well-defined and distinctive dimension scalings (7); however, this method is inadequate for heterogeneous materials systems,

particularly those with multiple competing types of active sites/ areas. Therefore, a direct mapping of the electrochemical activity with nanoscopic resolution and single-edge sensitivity is highly desired.

Nanoscale maps of catalytic activity have previously been obtained by in situ spectroscopic and single-molecule techniques (8– 12), scanning tunneling microscopy (7, 13), and various electrochemical scanning probe microscopy techniques, including scanning electrochemical microscopy (SECM) (14), scanning ion conductance microscopy (SICM) (15), scanning electrochemical cell microscopy (SECCM) (16), and plasmonic-based electrochemical current imaging (8). The spatial resolution of SECCM is currently 100-200 nm as limited by the size of the liquid meniscus contact area with the sample surface (16, 17), and higher resolution (15) can be attained in SICM with a nanopipette tip. It is worth noting that both SECCM and SICM techniques only map overall activity of the sample surface without measuring fluxes of specific products or detecting intermediates (18) of electrocatalytic reactions. In SECM, the reactivity of electrocatalysts is characterized by scanning a miniaturized electrode tip very close to the catalyst's surface (14,

Significance

A major challenge in electrocatalysis is pinpointing active sites on the surface, particularly when they are at the atomic scale. Direct electrochemical measurements of individual materials' edges have not yet been reported. Here we use the scanning electrochemical microscope (SECM) to independently image topography and local catalytic activity. The 15-nm spatial resolution and high sensitivity allowed us to distinguish the higher activities of the materials' edges from that of the fully coordinated surfaces *in operando*. The spatially resolved electrochemical information combined with state-of-the-art electron tomography that unravels the three-dimensional complexity of the edges and ab initio calculations revealed the intricate coordination-dependent catalytic activity of the Ni oxide nanosheet edge that is not accessible by other methods.

Author contributions: M.V.M., J.-C.Z., and H.L.X. designed research; T.S., D.W., M.V.M., H.C., J.-C.Z., R.M.R., F.L., and H.L.X. performed research; T.S., D.W., M.V.M., H.C., J.-C.Z., and H.L.X. analyzed data; and T.S., D.W., M.V.M., H.C., J.-C.Z., R.M.R., F.L., and H.L.X. wrote the paper.

The authors declare no conflict of interest.

This article is a PNAS Direct Submission.

Published under the PNAS license.

¹T.S. and D.W. contributed equally to this work.

²To whom correspondence may be addressed. Email: michael.mirkin@qc.cuny.edu, jczheng@xmu.edu.cn, or huolin.xin@uci.edu.

This article contains supporting information online at www.pnas.org/lookup/suppl/doi:10.1073/pnas.1821091116/-/DCSupplemental.

Published online May 24, 2019.

19-21). Due to the inherent selectivity of electrochemical experiments, the nanoelectrode tip can be used to measure local fluxes of the reactants and products and determine the rates of specific heterogeneous reactions in the nanoscale domains (22-24). The resolution is, however, limited by the tip size and diffusional broadening. Therefore, using a sufficiently small and well-shaped tip electrode is essential for nanoscopic imaging. Exploiting recent advances in fabrication of SECM nanotips (22, 23, 25, 26), here we used a well-characterized, polished nanodisk tip to directly image catalytic activity toward the OER over a semi-2D nickel oxide nanosheet with a sub-20 nm lateral resolution. (The word "direct" is used here in a sense that the measured tip current provides unambiguous quantification of the local electrochemical activity on the substrate surface under the tip.) By using two modes of the SECM operation, i.e., the feedback mode imaging with ferrocene methanol redox mediator and the generation/collection mode mapping of oxygen fluxes, it is possible to independently image the topography and reactivity of the same defect area. Taking advantage of the high spatial resolution of the nanotip and coupling the two SECM modes allowed us to establish that the catalytic activity for OER at the edge of the nickel oxide nanosheet is significantly higher than that of the basal plane, i.e., (111) surface of the nanosheet. To localize the atomic-scale active sites that can account for the activity increase at the edge, we interrogated the 3D atomistic details of the edges using electron tomography. The tomography reconstruction shows that the nickel oxide nanosheet is 10-20 nm thick and has an obtuse-angle double-beveled edge shape. Using the experimentally determined atomic structures as inputs, our ab initio calculations show that the (002) nanofacet of the edge is far more active than other components, such as the (111) facet and the (111)/(111) corner sites, and thus gives the enhanced OER current when the nanotip is scanned across the edge.

This work not only showcases the possibility of probing electrochemical signals over individual material edges, but also demonstrates that the strategy of combining ultrahigh-resolution SECM, electron tomography, and ab initio calculations provides a promising route for uncovering catalytic active sites on structurally complex electrocatalysts.

Results

Nio Nanosheet OER Catalysts. To interrogate the potentially active edge and corner sites, here we employ well-defined 2D NiO nanosheets that were prepared by the hydrothermal method (*SI Appendix*) (27). This synthesis method produces NiO nanosheets that are essentially flat, single-crystalline slabs containing hexagonal defect holes with well-defined edges (*SI Appendix*, Fig. S1). The thickness of the nanosheet is ~10–20 nm, and the size of defect holes ranges from tens to hundreds of nanometers.

High-Resolution SECM. In the SECM experiments, a small metal electrode (tip) is scanned over the substrate surface to map its topography and reactivity. Two complementary modes of the SECM operation are employed in this study to directly image the catalytic activity for the OER over a semi-2D nickel oxide nanosheet. In the feedback mode experiment (Fig. 1A), a nanometer-sized SECM probe was brought within a short distance from the NiO nanosheet immobilized on a flat, highly oriented pyrolytic graphite (HOPG) surface (SI Appendix). The electrolyte contained a redox mediator (ferrocenemethanol; Fc) and the tip potential (E_T) was such that the mediator oxidation occurred at a rate governed by diffusion. When the separation distance between the tip and substrate (d) is small enough (i.e., comparable to tip radius, a), the oxidized form of the mediator (Fc⁺) produced at the tip surface gets reduced at the substrate, and the tip current increases with decreasing d (positive feedback; the tip current near the surface is higher than its value in the bulk solution, $i_T > i_{T,\infty}$). If no mediator regeneration occurs at the substrate or the regeneration rate is slow, i_T decreases with decreasing d because of the hindered diffusion of

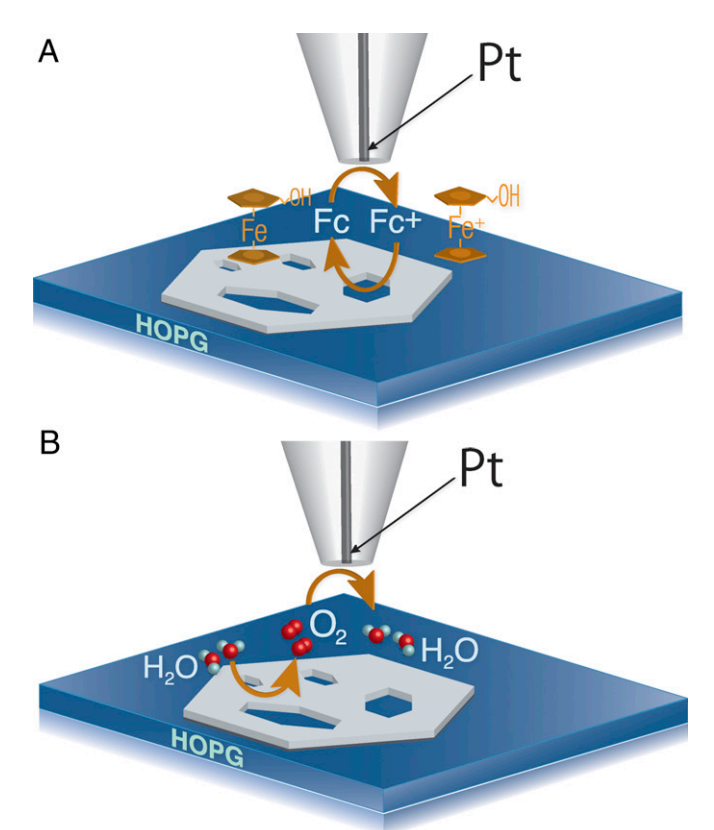


Fig. 1. SECM: schematic representation of (*A*) positive feedback produced by oxidation/reduction of ferrocenemethanol (Fc) and (*B*) substrate generation/tip collection of dioxygen at NiO nanosheet. The figure is not drawn to scale

Fc (negative feedback; $i_T < i_{T,\infty}$). Two experimental current vs. distance curves obtained over the NiO surface and over the HOPG exposed through the defect hole are shown in *SI Appendix*, Fig. S2. The defect holes in the NiO nanosheets could then be imaged based on the different mediator regeneration rates at the NiO and the underlying HOPG surface.

In substrate generation/tip collection mode (SG/TC mode; Fig. 1B), the tip collects the redox species generated at the substrate surface (e.g., O_2 in Fig. 1B). In our experiments, oxygen was produced at the catalytic NiO surface, but not at the inert HOPG (SI Appendix, Fig. S3). Thus, the higher tip current is expected above the NiO surface, and lower i_T —over the defects, which is exactly opposite to the feedback mode situation.

Fig. 24 shows a feedback mode image obtained by scanning an 80-nm-radius Pt tip over a NiO nanosheet. The size of the Pt tip was determined by atomic force microscopy and cyclic voltammetry (SI Appendix, Fig. S4). The slow reduction of Fc⁺ at the NiO semiconductor surface resulted in negative SECM feedback ($i_{T,\infty}$ = 23.7 pA). Significantly higher i_T can be seen over submicrometersized defect areas due to the rapid mediator regeneration at the exposed carbon surface. By contrast, the rate of the OER at the NiO surface is expected to be higher than at the catalytically inert HOPG. The SG/TC image of same substrate area (Fig. 2B) shows the higher O₂ reduction current over the portion of the substrate covered with NiO and the lower i_T over the defect holes exposing HOPG. The obtained catalytic activity map (Fig. 2B) is in good qualitative agreement with the feedback mode image (Fig. 2A), although the apparent defect size in the SG/TC image is somewhat larger because of the diffusional broadening effect (24). (The nonzero tip current over the HOPG surface is due to oxygen produced by water oxidation at the NiO substrate and accumulated in



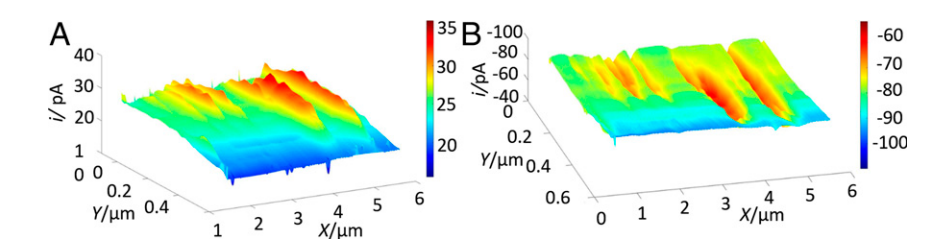


Fig. 2. SECM imaging of NiO nanosheet with defect holes: (A) Feedback mode and (B) SG/TC mode SECM images of the same portion of the NiO nanosheet with defect holes exposing the underlying HOPG. Solution contained 0.001 M KOH, 0.001 M Fc, and 0.1 M KCI. $E_T = (A)$ 0.5 and (B) -0.6 (V vs. Ag/AgCI). The substrate was either at (A) the open circuit potential or (B) biased at $E_S = 0.9$ V. a = 80 nm; $d \sim 80$ nm. Pixel density: $100/\mu$ m (x axis) and $25/\mu$ m (y axis).

solution.) The corresponding 2D color maps are shown in *SI Appendix*, Fig. S5.

More detailed images of the NiO/HOPG transition region were obtained by using a smaller Pt tip (a = 20 nm) to zoom in on the edge of a defect hole (Fig. 3; the corresponding 2D color maps are shown in *SI Appendix*, Fig. S6). A 200×200 -nm² feedback mode image (Fig. 3A) shows a smooth, continuous transition from the higher current produced by the Fc regeneration at the carbon surface to lower current over NiO (negative feedback), occurring over \sim 50–70-nm tip displacement along the x axis. In the SG/TC image of the same substrate area (Fig. 3B), the transition between the higher O_2 reduction current over NiO and lower i_T over the HOPG surface occurs over approximately the same ~50-70-nm distance, as can be seen from the line scan extracted from that image (Fig. 3C). However, unlike the smooth transition in Fig. 3A, this image contains a pronounced peak (at $x \sim 130$ nm), suggesting a significantly higher catalytic activity of the NiO edge toward oxygen evolution. The 10-20% current increase over the nanosheet edge was reproducible in line scans obtained with different tips and NiO samples (Fig. 3C and SI Appendix, Fig. S7). It is worth noting that diffusion broadening is somewhat reduced in Fig. 3C due to the shorter acquisition time. SI Appendix, Fig. S8 shows the analysis of the line scans over the HOPG/NiO boundary from SI Appendix, Fig. S7 that can be used to evaluate the lateral resolution of our reactivity maps. The line scans were deconvolved into a linear combination of a Gaussian function and a Z-shaped membership function. The lower bound of our resolution can be calculated by measuring the full width at half maximum of the Gaussian function. The full width averaged over the four scans is 16.5 ± 0.3 nm. This number is close to the 20-nm effective tip radius in Fig. 3 and SI Appendix, Fig. S7. It should be noted that our instrumental resolution is better than this number because the full-width measurement includes the width of the underlying (100) facet. Therefore, the attained spatial resolution is on the order of 15 nm.

Three-Dimensional Characterization of the Edge Structures. Using two modes of the SECM, we have independently mapped the topography and catalytic activity of a 2D NiO nanosheet with a nanoscale resolution. With the enhanced resolution and sensitivity, we were able to determine that the catalytic activity of a few-nanometer-wide area of NiO at the defect edge toward the OER is significantly higher than that of the NiO (111) basal surface. To understand the edge-enhanced activity with mechanistic details, we need to retrieve information regarding the atomic structures at these edges. We used electron tomography to reconstruct the 3D structures at the edges (see Methods for details). A tilt series of transmission electron microscopy (TEM) images of the NiO nanosheets was recorded from -70° to +70° with 1° tilt intervals and the tomograms were reconstructed with a multiplicative simultaneous iterative reconstruction technique (28). Fig. 4 shows the 3D rendition of such a semi-2D NiO with 3D complexities at the edges (also see Movies S1-S5). The NiO nanosheets are flat slabs with hexagonal holes with obtuse-angle double-beveled edges. With the help of aberration-corrected Zcontrast scanning TEM (STEM), we are able to verify that the top and bottom basal planes are a pair of {111} surfaces and the projected norm of the defect hole edges points toward the <112> direction (Fig. 4C, also see SI Appendix, Fig. S9). The reconstructions show that the edges are faceted. By measuring the angles between the facets and the basal planes, we determine that the two terminating nanofacets are {111} and {100} surfaces (experimental reconstruction shown in Fig. 4B and Movies S2–S5, and extracted atomic models shown in Fig. 4D and Movie S6). Basically, the edges are terminated with three additional

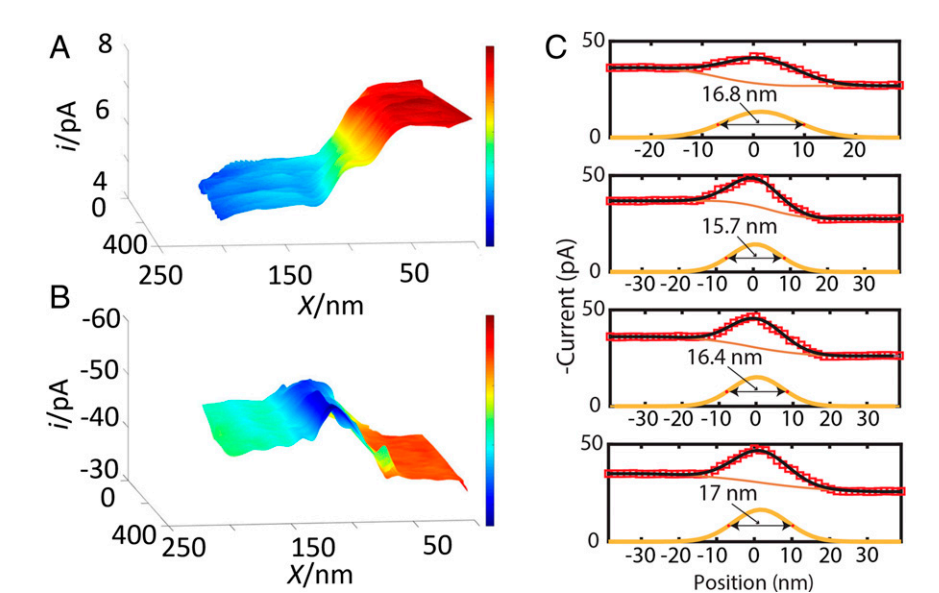


Fig. 3. SECM imaging of an edge: (A) feedback mode and (B) SG/TC SECM images of the NiO edge. Pixel density: 330/μm (x axis) and 100/μm (y axis). (C) Four experimental line scans across the NiO nanosheet edge recorded in the SG/TC mode. Tip radius, a \sim 20 nm. Solution contained 0.001 M KOH, 0.001 M Fc, and 0.1 M KCl. $E_{\rm T}=$ (A) 0.5 and (B) -0.6 (V vs. Ag/AgCl). The substrate was either at (A) the open circuit potential or (B) biased at $E_{\rm S}=$ 0.9 V.

coordination exposures that the basal planes do not have—{100} facet, the intersecting edge between {111} basal plane and {111} nanofacet, and the intersecting edge between {100} and {111} nanofacets.

Ab Initio Calculations. Different from 2D materials, where the edge structure can be simply interpreted as lower coordinated sites, in the case of our NiO nanosheets, the edges consist of more than one component that could contribute to the edge-enhanced activity. To unravel which one(s) are responsible for the higher activity, we employed the density functional theory calculation using the generalized gradient approximation (GGA) at the Perdew–Burke–Ernzerhof (PBE) level with spin-orbital approximation. In our calculations, we considered the (100), (111) plane, (111)/(111), (111)/(100) edge of NiO. A (2 \times 2) coverage for surface and (2 \times 2) coverage for edge calculation with a vacuum layer of 18 Å along the nonperiodic direction was used to calculate the O*, HO*, and HOO* adsorptions on the surfaces and edges (see *Methods* for details).

Fig. $5\,B$ and C plot the calculated the free energy for each step of the four-electron reaction pathway. Fig. 5B shows that among the four types of surfaces/edge terminations, the (100) surface has the lowest overpotential. When a bias of 1.57 V is applied (the same potential was used in the SECM experiment), we find that only on the (100) surface the reaction free energy continues in the downward direction, while reactions on the (111) surface, the (111)/(111) edge, and the (111)/(100) edge meet a significant upward barrier at the O* to HOO*, HO* to O*, and the HOO* to O2 steps, respectively. Fig. 5D shows the OER volcano plot which places the NiO (100) surface on the top of the curve with the (111)/(111) and (111)/(100) edges following and (111) surface performing the poorest among the three. Based on this analysis, we can conclude, with a high degree of confidence,

that the (100) nanofacet at the edge is responsible for the catalytic enhancement seen in the SECM measurement.

The above calculations predict that the OER overpotential at the NiO (111) surface is significantly higher than that at the NiO edge; thus, a large difference in their reactivities can be expected. However, only a modest (10–20%) increase in the tip current over the NiO edge can be seen in Fig. 3B and SI Appendix, Fig. S7. These experimental and theoretical results were reconciled by finite-element simulations of the SG/TC SECM experiments (see *SI Appendix* for details). Four line scans of the 20-nm-radius tip over the NiO edge are simulated in Fig. 6 for different ratios of the OER current densities at the basal plane and at the edge. From Fig. 6, the current density at the edge has to be \sim 200 times higher than at the NiO basal surface for the maximum tip current increase over the edge of 18% (green curve), similar to that observed experimentally. One should notice that the line scan simulated assuming no catalytic enhancement at the edge (black curve in Fig. 6) exhibits a smooth, continuous transition from the carbon surface to NiO without any peak over the edge. Thus, the peak observed in the experimental images and line scans (Fig. 3 B and C) cannot be attributed to the additional surface area at the edge due to the finite thickness of the nanosheet (15 nm in Fig. 6).

All line scans in Fig. 6 were simulated with the current density of 50 mA/cm² at the NiO basal plane. This value is comparable to that reported (30) for the NiO nanosheet at +1.57 V vs. reversible hydrogen electrode and corresponds to the tip current over NiO in a reasonable agreement with the experiment. However, some experimental issues, such as the nonzero background current due to the oxygen production at a macroscopic NiO substrate and Fc contribution to SG/TC signal, have not been included in these simulations. Another inevitable simplifying assumption is a constant OER current density on the nanosheet

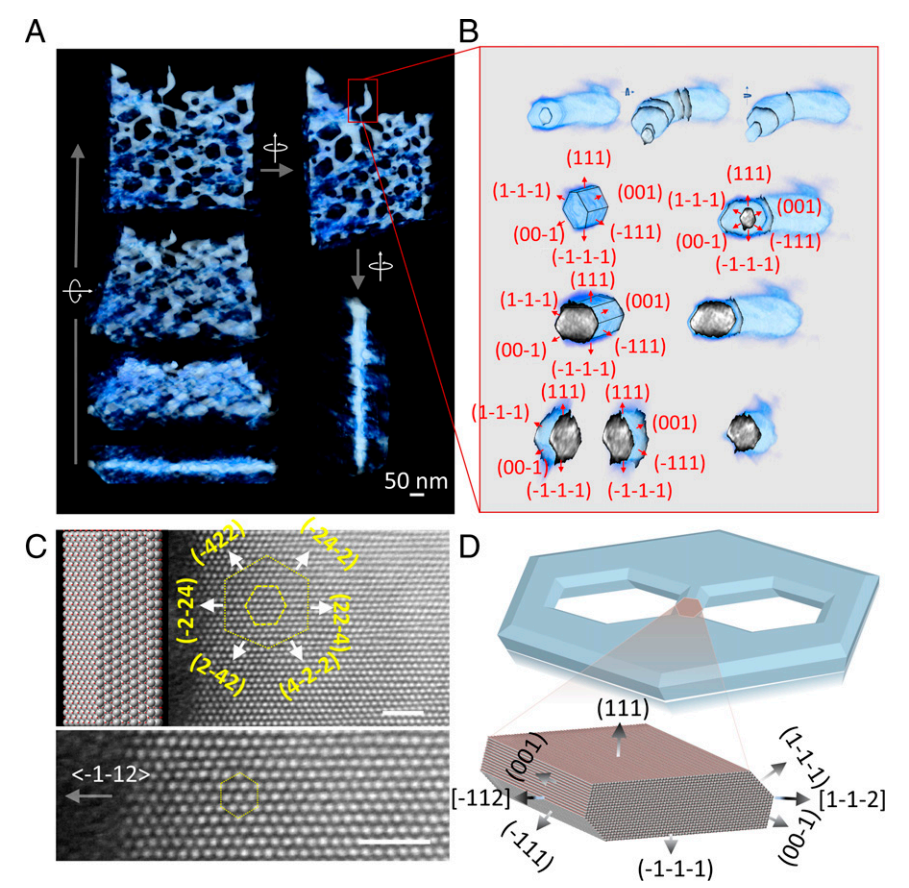


Fig. 4. Three-dimensional structures of the edge. (A) Overview and (B) a close-up view of the NiO nanosheet reconstructed by electron tomography (also see Movies S1–S5). (C) Atomic-resolution Z-contrast STEM imaging of the nanosheet when it is laid down flat. The image shows the flat basal plane of the nanosheet is a (111) surface and the edges point toward the <112> direction which is in agreement with the (001)/(–111) facet decomposition as shown in B and C. (D) A computer-generated model of the nanosheet and the 3D atomistic model of the edges. (Scale bars in C are 1 nm.)



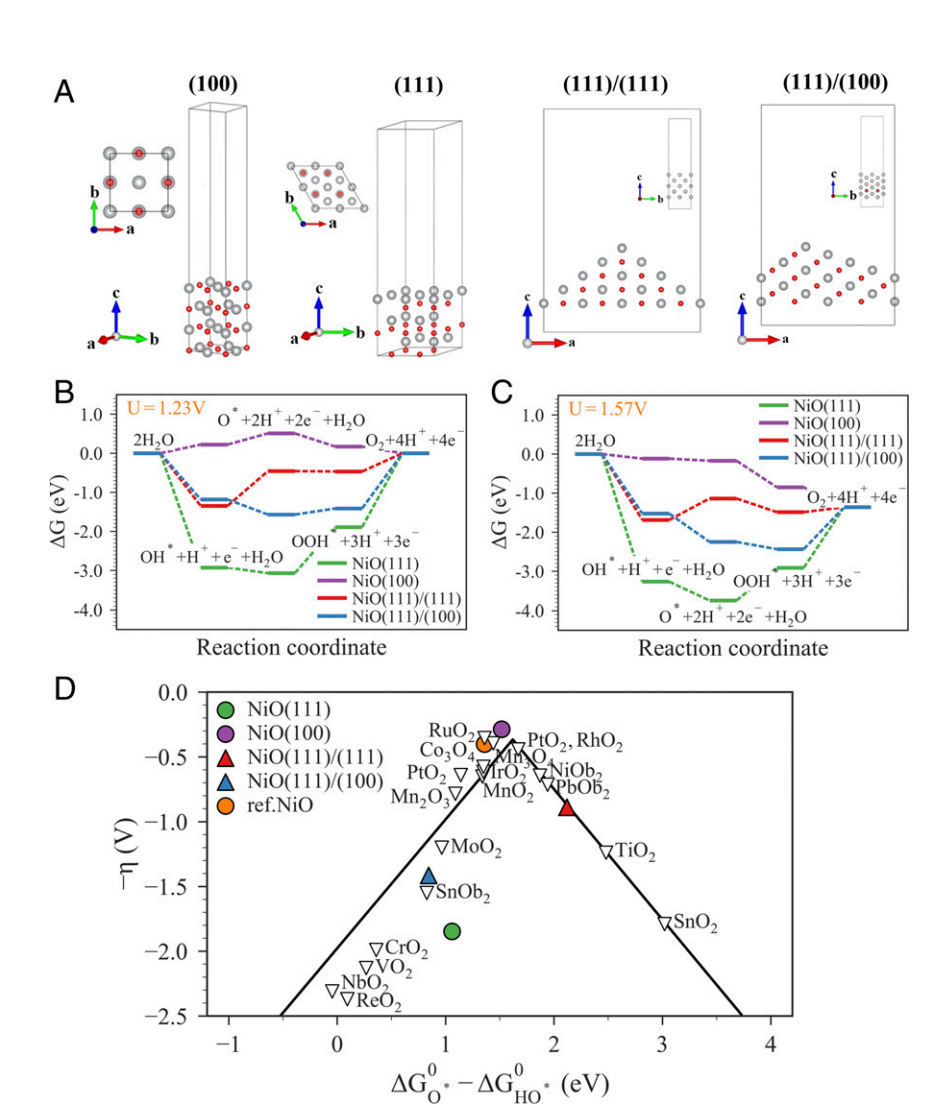


Fig. 5. Ab initio calculation of the OER reaction kinetics. (A) The four types of atomic terminations calculated. (B and C) Standard free-energy diagram for the OER at (B) equilibrium potential for oxygen evolution (U = 1.23 V) and (C) the experimentally applied potential (U = 1.57 V). (D) The activity volcano plot. Data from ref. 29.

edge, which should actually vary for different nanofacets (Figs. 4 and 5).

In addition, the simulation result allows us to estimate the impact of the defects on the OER activity. Let us consider a hypothetical 1-µm-diameter circular defect in a 15-nm-thick NiO sheet. The current density of the OER on the basal plane is $\sim\!50~\text{mA/cm}^2$, and the activity of the edge area is $\sim\!10,000~\text{mA/cm}^2$. Then, the total OER current produced by the 15-nm-thick edge of this defect is $\sim\!2\pi\times0.5~\text{µm}\times15~\text{nm}\times10,000~\text{mA/cm}^2=4.7~\text{nA}$. If no defect was present, the total OER current produced on the same 1-µm-diameter circular area of the basal NiO sheet is $\pi\times(0.5~\text{µm})^2\times50~\text{mA/cm}^2=0.39~\text{nA}$. The additional current due to the presence of a 1-µm-diameter circular defect is $\sim\!4.3~\text{nA}$, corresponding to $\sim\!12\text{-fold}$ increase in the effective OER rate. The smaller the defect, the more significant the current increase per unit area.

Conclusion

Discovering and understanding active sites on the surface of a realistic/heterogeneous electrocatalyst is essential for the design and synthesis of next-generation catalysts with optimized activity. In this work, we show that by optimizing the electrodes and the imaging method it is possible for SECM to visualize the OER activity of a NiO catalyst with an unprecedented sub-20-nm resolution and single-edge sensitivity. This allowed us to locate the active sites at the NiO materials' edges. Using electron tomography, which resolves the 3D complexities of the edges, in

conjunction with ab initio calculations, we found that the (100) nanofacet is responsible for ~200-fold enhancement of activity at the edge. In addition to showing the possibility of probing electrochemical signals over individual material edges, this work demonstrated that combining ultrahigh-resolution SECM, electron tomography, and ab initio calculation is a viable strategy for revealing catalytic active sites on structurally complex electrocatalysts.

Methods

SECM. The Pt nanoelectrode tips were fabricated by heat-sealing commercially available Pt microwire into the glass capillary, as described previously (31). (See *SI Appendix* for details of tip preparation and characterization.) NiO nanosheets were dispersed in methanol under sonication and then drop casted on the HOPG surface. After drop casting, the voltammograms of the substrate and the i_T vs. E_S curves were obtained to optimize the imaging conditions (see *SI Appendix* for details).

The SECM experiments were carried out with a home-built instrument described previously (32). To avoid crashing, the tip electrode was first positioned about 100 μm above the HOPG/NiO substrate using a long-distance video microscope and then moved toward the substrate by the piezo scanner. The tip current was collected during the subsequent fine approach or imaging (see SI Appendix for further details). The outer-sphere redox mediator (Fc) was added to solution for feedback mode SECM imaging (Fig. 1A). Due to the low density of drop-casted NiO, bare HOPG surface exposed to solution constituted a significant fraction of the substrate. Thus, the open circuit potential of the unbiased substrate was determined by the reduced Fc species present in solution, and therefore was significantly more negative than the standard potential of Fc (see ref. 18 for discussion). The concentration of Fc was low (1 mM) to minimize its effect on SG/TC experiments.

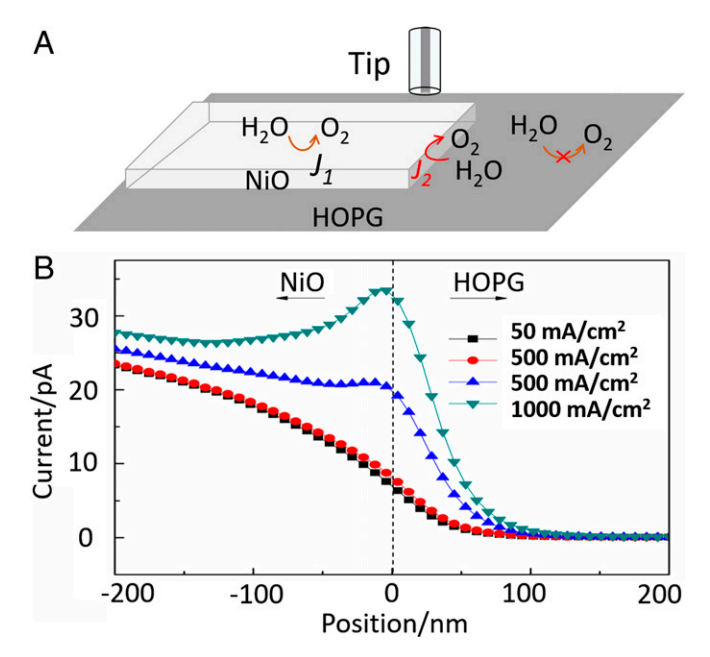


Fig. 6. Schematic representation of the simulation of the OER at the NiO basal plane and edge under SG/TC SECM conditions (A) and simulated line scans across the NiO edge at different edge/basal plane activity ratios (B). The thickness of the NiO nanosheet is 15 nm. The OER current density at the basal plane, $J_1 = 50 \text{ mA/cm}^2$. The edge current density values (J_2) are shown for each simulated curve. The 0-nm position (dashed line) corresponds to the NiO edge. a = 20 nm; d = 20 nm.

Finite-element simulations were carried out using COMSOL Multiphysics version 5.2 commercial simulation package (see SI Appendix for details). TEM and electron tomography. The high-resolution annular dark-field STEM imaging of the NiO thin slabs was performed using a probe-corrected cold-

- 1. W. Bao et al., Mapping local charge recombination heterogeneity by multidimensional nanospectroscopic imaging. Science 338, 1317-1321 (2012).
- 2. I. L. Buurmans, B. M. Weckhuysen, Heterogeneities of individual catalyst particles in space and time as monitored by spectroscopy. Nat. Chem. 4, 873-886 (2012).
- 3. S. Berweger et al., Optical nanocrystallography with tip-enhanced phonon Raman spectroscopy. Nat. Nanotechnol. 4, 496-499 (2009).
- 4. C. C. L. McCrory, S. Jung, J. C. Peters, T. F. Jaramillo, Benchmarking heterogeneous electrocatalysts for the oxygen evolution reaction. J. Am. Chem. Soc. 135, 16977-16987 (2013).
- 5. O. Diaz-Morales, D. Ferrus-Suspedra, M. T. M. Koper, The importance of nickel oxyhydroxide deprotonation on its activity towards electrochemical water oxidation. Chem. Sci. 7, 2639-2645 (2016).
- 6. Y. Zhao et al., Ultrafine NiO nanosheets stabilized by TiO2 from monolayer NiTi-LDH precursors: An active water oxidation electrocatalyst. J. Am. Chem. Soc. 138, 6517-6524 (2016).
- 7. T. F. Jaramillo et al., Identification of active edge sites for electrochemical H2 evolution from MoS2 nanocatalysts. Science 317, 100-102 (2007).
- 8. X. Shan et al., Imaging the electrocatalytic activity of single nanoparticles. Nat. Nanotechnol. 7, 668-672 (2012).
- 9. S. Nie, S. R. Emory, Probing single molecules and single nanoparticles by surfaceenhanced Raman scattering. Science 275, 1102-1106 (1997).
- 10. J. B. Sambur et al., Sub-particle reaction and photocurrent mapping to optimize catalyst-modified photoanodes. Nature 530, 77-80 (2016).
- 11. C.-Y. Wu et al., High-spatial-resolution mapping of catalytic reactions on single particles. Nature 541, 511-515 (2017).
- 12. W. Xu, J. S. Kong, Y.-T. E. Yeh, P. Chen, Single-molecule nanocatalysis reveals heterogeneous reaction pathways and catalytic dynamics. Nat. Mater. 7, 992-996 (2008).
- 13. J. H. K. Pfisterer, Y. Liang, O. Schneider, A. S. Bandarenka, Direct instrumental identification of catalytically active surface sites. Nature 549, 74-77 (2017).
- 14. A. J. Bard et al., Chemical imaging of surfaces with the scanning electrochemical microscope. Science 254, 68-74 (1991).
- 15. M. Kang et al., Simultaneous topography and reaction flux mapping at and around electrocatalytic nanoparticles. ACS Nano 11, 9525-9535 (2017).
- 16. C. L. Bentley et al., Electrochemical maps and movies of the hydrogen evolution reaction on natural crystals of molybdenite (MoS₂): Basal vs. edge plane activity. Chem. Sci. 8. 6583-6593 (2017).
- 17. X. Feng, K. Jiang, S. Fan, M. W. Kanan, Grain-boundary-dependent CO2 electroreduction activity. J. Am. Chem. Soc. 137, 4606-4609 (2015).
- 18. M. Zhou, Y. Yu, K. Hu, M. V. Mirkin, Nanoelectrochemical approach to detecting short-lived intermediates of electrocatalytic oxygen reduction. J. Am. Chem. Soc. 137, 6517-6523 (2015).

field-emission dedicated STEM operated at 200 keV. TEM tomography tilt series acquisition was performed in FEI Talos F200X operated at 200 keV. Images were acquired from -70° to +70° with 2° tilt intervals. The 3D tomograms were reconstructed by a home-written MATLAB code implementing the multiplicative simultaneous iterative reconstruction technique and visualized by Avizo (28).

Ab initio calculations. First-principle calculations were carried out using the density functional theory (DFT) implemented in the QUANTUM ESPRESSO package (33). The GGA in PBE form and Ultrasoft pseudopotentials with spin-orbital approximation are employed. The kinetic energy cutoff for plane wave and charge density are 40 and 400 Ry, respectively. The (100), (111) plane and (111&111), (100&111) edge of NiO were considered. A 2×2 coverage surface and edge with a vacuum space of 18 Å along the nonperiodic direction were used to perform the catalytic property calculation. In addition, the Brillouin zone was sampled using a Monkhorst-Pack $4 \times 4 \times 1$ for surface and edge calculation. The lattice constant of NiO was calculated

The OER mechanism includes four electron reaction paths (34):

$$H_2O + * = HO^* + H^+ + e^-,$$
 [1]

$$HO^* = O^* + H^+ + e^-, \qquad [2]$$

$$O^* + H_2O \leq HOO^* + H^+ + e^-,$$
 [3]

$$HOO^* = * + O_2 + H^+ + e^-.$$
 [4]

The free energy for each step was calculated as $\mu = E_{DFT} + ZPE - TS$, where E_{DFT} is the total energy calculated by DFT and ZPE is the zero point energy estimated under harmonic approximation by taking the vibrational frequencies of adsorbates or molecules as calculated within DFT.

ACKNOWLEDGMENTS. This work was supported by the National Science Foundation, CHE-1900463 (to M.V.M.) and CHE-1900401 (to H.L.X.). H.C. and J.-C.Z. were supported by the National Natural Science Foundation of China (Grant 51661135011) and Xiamen University Malaysia Research Fund (Grant XMUMRF/2019-C3/IORI/0001). This research used resources of the Center for Functional Nanomaterials, which is a US Department of Energy Office of Science Facility, at Brookhaven National Laboratory under Contract DE-SC0012704.

- 19. D. V. Esposito, I. Levin, T. P. Moffat, A. A. Talin, H2 evolution at Si-based metalinsulator-semiconductor photoelectrodes enhanced by inversion channel charge collection and H spillover. Nat. Mater. 12, 562-568 (2013).
- 20. C. Tan et al., Reactivity of monolayer chemical vapor deposited graphene imperfections studied using scanning electrochemical microscopy. ACS Nano 6, 3070-3079 (2012).
- 21. J. Rodríguez-López et al., Quantification of the surface diffusion of tripodal binding motifs on graphene using scanning electrochemical microscopy. J. Am. Chem. Soc. **134**, 6224-6236 (2012).
- 22. S. Amemiya, Electroanalytical Chemistry: A Series of Advances, A. J. Bard, C. G. Zoski, Eds. (CRC Press, 2015), vol. 26, pp. 1-72.
- 23. T. Sun, Y. Yu, B. J. Zacher, M. V. Mirkin, Scanning electrochemical microscopy of individual catalytic nanoparticles. Angew. Chem. Int. Ed. Engl. 53, 14120-14123 (2014).
- 24. J. Rodríguez-López, C. G. Zoski, A. J. Bard, Scanning Electrochemical Microscopy (CRC Press, ed. 2, 2012), pp. 525-568.
- 25. P. Y. Blanchard et al., Scanning electrochemical microscopy study of permeability of a thiolated aryl multilayer and imaging of single nanocubes anchored to it. Langmuir **32**, 2500-2508 (2016).
- 26. J. Kim et al., Electrocatalytic activity of individual Pt nanoparticles studied by nanoscale scanning electrochemical microscopy. J. Am. Chem. Soc. 138, 8560-8568 (2016).
- 27. J. C. Hu et al., Preparation and surface activity of single-crystalline NiO(111) nanosheets with hexagonal holes: A semiconductor nanospanner. Adv. Mater. 20, 267-271 (2008).
- 28. P. A. Midgley, M. Weyland, 3D electron microscopy in the physical sciences: The development of Z-contrast and EFTEM tomography. Ultramicroscopy 96, 413-431 (2003).
- 29. J. K. Nørskov et al., Origin of the overpotential for oxygen reduction at a fuel-cell cathode. J. Phys. Chem. B 108, 17886-17892 (2004).
- 30. Y. Xu et al., Facile fabrication method for ultrathin NiO/Ni nanosheets as a highperformance electrocatalyst for the oxygen evolution reaction. RSC Adv. 7, 18539-18544 (2017)
- 31. P. Sun, M. V. Mirkin, Kinetics of electron-transfer reactions at nanoelectrodes. Anal. Chem. 78, 6526-6534 (2006).
- 32. Y. X. Wang, K. Kececi, J. Velmurugan, M. V. Mirkin, Electron transfer/ion transfer mode of scanning electrochemical microscopy (SECM): A new tool for imaging and kinetic studies. Chem. Sci. 4, 3606-3616 (2013).
- 33. P. Giannozzi et al., QUANTUM ESPRESSO: A modular and open-source software project for quantum simulations of materials. J. Phys. Condens. Matter 21, 395502 (2009).
- 34. I. C. Man et al., Universality in oxygen evolution electrocatalysis on oxide surfaces. ChemCatChem 3, 1159-1165 (2011).